Organelle trafficking of chimeric ribozymes and genetic manipulation of mitochondria

Romain Val[1], Eliza Wyszko[2], Clarisse Valentin[1], Maciej Szymanski[2], Anne Cosset[1], Malek Alioua[1], Theo W. Dreher[3], Jan Barciszewski[2] and André Dietrich[1,*]

[1]Institut de Biologie Moléculaire des Plantes, CNRS and Université de Strasbourg, 12 rue du Général Zimmer, 67084 Strasbourg, France, [2]Institute of Bioorganic Chemistry, Polish Academy of Sciences, Noskowskiego 12/14, 61-704 Poznan, Poland and [3]Department of Microbiology, Oregon State University, Corvallis, Oregon 97331-3804, USA

ABSTRACT

With the expansion of the RNA world, antisense strategies have become widespread to manipulate nuclear gene expression but organelle genetic systems have remained aside. The present work opens the field to mitochondria. We demonstrate that customized RNAs expressed from a nuclear transgene and driven by a transfer RNA-like (tRNA-like) moiety are taken up by mitochondria in plant cells. The process appears to follow the natural tRNA import specificity, suggesting that translocation indeed occurs through the regular tRNA uptake pathway. Upon validation of the strategy with a reporter sequence, we developed a chimeric catalytic RNA composed of a specially designed *trans*-cleaving hammerhead ribozyme and a tRNA mimic. Organelle import of the chimeric ribozyme and specific target cleavage within mitochondria were demonstrated in transgenic tobacco cell cultures and *Arabidopsis thaliana* plants, providing the first directed knockdown of a mitochondrial RNA in a multicellular eukaryote. Further observations point to mitochondrial messenger RNA control mechanisms related to the plant developmental stage and culture conditions. Transformation of mitochondria is only accessible in yeast and in the unicellular alga *Chlamydomonas*. Based on the widespread tRNA import pathway, our data thus make a breakthrough for direct investigation and manipulation of mitochondrial genetics.

INTRODUCTION

In eukaryotic cells, mitochondria ensure fundamental functions in energy production, redox processes, metabolic pathways and apoptosis. The genetic system present in these cytoplasmic organelles is thus of primary relevance for cell survival. The mammalian mitochondrial DNA is a small and compact molecule of 16.5 kb containing no intergenic regions or introns (1). Gene expression driven by promoters located in the single non-coding region involves a number of specific transcriptional and post-transcriptional steps (2). Higher plant mitochondria possess large genomes in which over half of the sequences are unassigned (3), but there is no reverse genetics approach available to probe for function. Plant mitochondrial gene expression is complex, including *cis*- and *trans*-splicing of introns (4), RNA processing and surveillance (5), as well as RNA editing (6). Many aspects of mitochondrial genetic processes remain to be investigated. Organelles also talk to the nucleus through retrograde signaling, but the nature of the underlying cascade that relays the information is largely unknown (7–9) and mitochondrial regulation mechanisms as a whole are still elusive. Mutations in the human organelle genome cause severe neurodegenerative diseases that are currently incurable (10). In plants, the mitochondrial genome is the source of cytoplasmic male sterility (CMS), a trait of major interest to crop breeders for hybrid generation (11). Genetic interactions between the organelles and the nucleus were reported to affect a number of other important agronomical traits, including yield, heterosis, combining ability, selfing rate, disease resistance and temperature or drought tolerance (12–14). The mechanisms underlying these cytoplasmically inherited effects are still largely unexplored and in many cases the respective roles of mitochondrial and chloroplastic genetics remain to be established.

Progress in the understanding of mitochondrial genetic processes and regulation pathways, as well as development of suitable gene technologies, are hindered by the lack of molecular approaches to manipulate and control the genetic system in these organelles. Chloroplast transformation was established more than two decades ago, first in

the unicellular alga *Chlamydomonas reinhardtii* (15) and subsequently in tobacco (*Nicotiana tabacum*) (16), based on biolistic-mediated transfection and homologous recombination of the transfected DNA with the resident plastid DNA. Episomal maintenance was later demonstrated, using a shuttle vector carrying a plastid origin of replication (17). Transplastomic plants have significantly contributed to the understanding of chloroplast gene expression, RNA editing or functional processes and the strategy has now entered biotechnological applications (18–21). In contrast, mitochondria are still amenable to genetic transformation only in yeast and *C. reinhardtii* (22,23). In this respect, we present here a major breakthrough for organelle genetics.

In the last decade, RNA-based strategies have become approaches of choice to silence eukaryotic genes and have been quite successful. However, there has been no indication that RNA interference, or a similar mechanism, would operate in organelles, as such pathways require a complex endogenous machinery. On the other hand, catalytic RNAs carry their own activity but they have to be adapted to the expected cellular context. Both approaches anyway need to target customized RNAs into the organelles. As a critical progress, the present work answers two of these questions. First, we have developed nuclear expression and organelle import of customized RNA sequences. In many organisms, including mammals, the mitochondrial genome does not code for a complete set of transfer RNAs (tRNAs), so that nuclear-encoded tRNAs are taken up from the cytosol (24,25). The process applies to one third to one half of the organelle tRNAs in higher plants. We demonstrate here that 'passenger' RNAs driven by a tRNA mimic can be translocated into mitochondria in plant cells. Second, we have designed and functionally validated *in vitro* a composite RNA bringing together a *trans*-cleaving ribozyme and a tRNA-like structure (TLS). Subsequent expression in plant cell suspensions and whole plants from a nuclear transgene established that this chimeric catalytic RNA was imported into the organelles and that the ribozyme moiety was active inside mitochondria. Furthermore, ribozyme-mediated cleavage triggered a drastic decrease in the level of the target, leading to the first directed RNA knockdown in the mitochondria of a multicellular eukaryote. Our results thus open new horizons for genetic investigation and functional manipulation of these organelles in living cells.

MATERIALS AND METHODS

Bioinformatic methods

The linker (L) to provide spacing between the hammerhead and PKTLS motifs in the chimera was selected from a pool of random sequences. The selection was based on predictions of RNA secondary structures using MFOLD (26). The candidate was chosen on the basis of its inability to form stable structures that would interfere either with PKTLS formation or hammerhead binding to the target sequence.

Gene constructs

Primer sequences are given in Supplementary Data and Supplementary Table S1. To generate a construct expressing the PSTY passenger sequence with the PKTLS tRNA mimic and the cHDV *cis*-ribozyme, two successive PCR reactions were carried out. The cHDV sequence was first amplified from a pre-existing recombinant plasmid (27) with the TLS-HDV5P direct primer, carrying an extension corresponding to the 3′-end of the PKTLS, and the HDV3PX reverse primer containing an XbaI site. Together with the TLS5PB direct primer containing a BamHI site, the resulting product served as a 'mega-primer' in a second PCR reaction which used as a template the pTYMC plasmid carrying the full TYMV genomic sequence (28). The second PCR created a fusion between the sequence of the last 186 nt (positions 6134–6318) of the TYMV genome (accession number X16378) and the sequence of the cHDV *cis*-ribozyme (27). The obtained fragment was subsequently inserted into the pCK-GFPS65C plasmid [i.e. the pRTL2 expression vector (29) containing the GFPS65C gene (30)] between the BamHI and XbaI sites located 3′ to the GFP sequence, yielding the pCKGFPS65C-PSTYPKTLScHDV plasmid. The latter was digested with XhoI and BamHI, so as to eliminate the translation leader and the GFP gene still present at that stage. The sticky ends were filled with the Klenow fragment of *Escherichia coli* DNA polymerase I and the DNA was re-circularized. The resulting pCK-PSTYPKTLScHDV plasmid was finally digested with HindIII and the whole expression cassette (CaMV 35S promoter, PSTYPKTLScHDV sequence, 35S terminator) was cloned into the HindIII site of the binary vector pBI101 (Clontech), generating the pBI-PSTYPKTLScHDV plasmid. The sequence differences in the PKTLSmet mutated variant versus the original PKTLS are located outside of the above primers. An identical strategy was thus developed to generate the pBI-PSTYPKTLSmetcHDV construct, taking in this case as starting template the pTYMC-U55/C54/A53(L1 = UU) plasmid (31) which carries the TYMV cDNA with the relevant mutations to confer a methionine specificity to the PKTLS.

For the catalytic RNA strategy, the complete sequence encoding the Rzatp9 *trans*-ribozyme, the linker L, the PKTLS and the cHDV *cis*-ribozyme was assembled by PCR amplification from the pCK-PSTYPKTLScHDV plasmid with the direct primer RzLTLS5PH containing a HindIII site and the reverse primer HDV3PE containing an EcoRI site. The obtained product was introduced into the HindIII and EcoRI sites of the pUCAP vector (32), re-excised with the AscI and PacI enzymes and finally cloned into the AscI and PacI sites of the inducible transcription unit of the pER8 vector (33), generating the pER8-Rzatp9LPKTLScHDV plasmid.

Nuclear transformants

Plasmids encoding the passenger RNAs, PKTLS and cHDV *cis*-ribozyme were used to transform *Nicotiana tabacum* BY-2 cells via *Agrobacterium tumefaciens*

following standard procedures (34). Transformed calli were selected on solid medium with kanamycin (pBI derivatives) or hygromycin (pER8 derivatives) and dispersed in liquid medium to generate transformed cell suspensions. For transgene expression, cells were subcultured in estradiol-supplemented liquid medium.

Plasmids carrying the gene constructs served in turn to transform *Arabidopsis thaliana* (Col-0) plants via *A. tumefaciens* through floral dip (35). Seeds were collected and germinated on solid agar medium containing hygromycin for selection. Antibiotic-resistant plants were grown further in the greenhouse to obtain next generation seeds. Homozygous transformants were used for Rzatp9-L-PKTLS RNA expression and *atp9* mRNA knockdown analysis. Plants were grown on solid agar medium which was overlaid with estradiol-supplemented liquid medium for transgene induction. Alternatively, plants grown on solid agar were transferred to culture plates containing liquid medium supplemented with estradiol and the roots were dipped into the medium.

Isolation of mitochondria

Protoplasts derived from BY-2 cells were resuspended in extraction buffer (0.3 M sucrose, 30 mM sodium diphosphate, 2 mM EDTA, 0.3% w/v BSA, 0.8% w/v polyvinyl pyrrolidone 25 K, 0.05% w/v cysteine, 5 mM glycine, 2 mM β-mercaptoethanol, pH 7.5) and disrupted by three passages through a 30-μm mesh nylon net (Scrynel, ZBF, Rüschlikon, Switzerland). Mitochondria were further isolated according to Delage *et al.* (36) using discontinuous Percoll (Sigma) gradients. Prior to RNA extraction, purified organelles were incubated in buffer containing 100 μg/ml RNase A and 750 U/ml RNase T1, re-isolated on Percoll gradients and washed with buffer containing 5 mM EDTA and 5 mM EGTA.

RNA extraction

Total RNA was extracted from *N. tabacum* cell suspensions and *A. thaliana* plants following standard TRI Reagent protocols (Molecular Research Center). To prepare organelle RNA, RNase-treated mitochondria (1–5 mg protein) were resuspended in 200 μl extraction buffer (Tris–HCl 10 mM pH 7.5, $MgCl_2$ 10 mM, SDS 1% w/v). After 2 min of vigorous shaking, the suspensions were centrifuged for 10 min at 10 000g. The supernatant was phenol extracted and nucleic acids were ethanol precipitated. The DNA was finally eliminated through several successive DNase treatments.

Reverse transcription, RT–PCR and CR–RT–PCR

Reverse transcription was carried out with SuperScript III (Invitrogen) using 2 pmol of a specific primer (Supplementary Data and Supplementary Table S1) or 250 ng of a random hexanucleotide mixture. Reactions were stopped by 15 min incubation at 70°C and the RT samples served directly for standard or real-time PCR. Standard RT–PCR products were analyzed on agarose gels, cloned into pGEM-T easy (Promega) and sequenced.

Prior to circularized RNA RT–PCR (CR–RT–PCR), the cap was removed with tobacco acid pyrophosphatase (Epicentre Biotechnologies). After phenol extraction and ethanol precipitation, RNA circularization was carried out with T4 RNA ligase (Fermentas). Reverse transcription through the junction between the 5′- and 3′-end of the RNAs of interest was performed with a direct primer in the PKTLS sequence. The cDNA was used as a template for a first PCR with the same primer and a primer in the passenger sequence, which was followed by a nested PCR. The final products were cloned into pGEM-T easy and sequenced.

Templates for *in vitro* synthesis of the *atp9* target RNAs and ribozyme chimeras

Primer sequences are given in Supplementary Data and Supplementary Table S1. DNA fragments corresponding to nucleotides 31–130 of the *A. thaliana atp9*-coding sequence (positions 278 895–279 152 in the complete mitochondrial genome with the accession number Y08501), or nucleotides 15–160 of the *N. tabacum atp9*-coding sequence (nucleotides 145 758–145 991 in the complete mitochondrial genome with the accession number NC_006581) were PCR amplified from *A. thaliana* or *N. tabacum* DNA using the primer pairs Atcibatps/Atcibatpas and Ntcibatps/Ntcibatpas, respectively. The direct primers contained the T7 RNA polymerase promoter. The DNA template for the synthesis of the Rzatp9-L-PKTLS RNA was constructed through two successive PCR steps. The first reaction was run with the primer pair linatps/TLS3P using the pCK-PSTYPKTLScHDV plasmid as a template. This step allowed joining the linker sequence to the PKTLS. The product of the first PCR was used as a template for a second amplification with the primer pair rzatps/TLS3P, joining the T7 promoter and ribozyme sequence to the linker already attached to the PKTLS. The DNA template for the synthesis of the extRzatp9-L-PKTLS RNA was amplified in a single PCR step with the primer pair ext5P/TLS3P taking the pER8-Rzatp9LPKTLScHDV plasmid as a template. The direct primer ext5P was carrying the T7 promoter sequence. Final PCR products to be used as templates for transcription were purified on Sephadex G-50 spin columns.

In vitro ribozyme cleavage assays

The *atp9* target RNAs and ribozyme chimeras were synthesized *in vitro* from the PCR constructs with T7 RNA polymerase and a RiboMAX kit (Promega). Radiolabeled target RNAs were obtained by including [α-^{32}P]UTP (800 Ci/mmol) into the reaction medium. Following transcription, DNA templates were hydrolyzed with RNase-free DNase (1 U, 15 min at 37°C). Transcripts were purified by phenol and chloroform extraction, gel-filtered on Sephadex G-50 spin columns and quantified by UV-absorbance measurement. The Rzatp9 RNA comprising only the *trans*-ribozyme was from Eurogentec.

Cleavage reactions containing 15 nM of unlabeled target RNA, 50 fmol (30 000 cpm) of labeled target RNA, 150 nM of ribozyme or ribozyme-L-PKTLS chimera, in 50 mM Tris–HCl pH 7.5 were incubated at 25°C for 1–5 h. Prior to the cleavage reaction, the target RNA

and catalytic RNA were usually denatured for 2 min at 75°C and slowly cooled down to 25°C to release the RNA structures resulting from the fast T7 RNA polymerase *in vitro* transcription. Cleavage products were fractionated on denaturing polyacrylamide gels and visualized by autoradiography.

Real-time PCR

Real-time PCR reactions were run on an iCycler (BioRad). Primers (Supplementary Data and Supplementary Table S1) were designed with the PrimerExpress software (Applied Biosystems). Their efficiency was verified with the LinRegPCR software (37) (bioinfo@amc.uva.nl). Real-time PCR was carried out in 20 µl samples containing 10 µl SybrGreen kit (MasterMix Plus, Eurogentec), 0.6 µM direct and reverse primer and 1 µl RT reaction (performed with a random hexanucleotide mixture). The following steps were applied: one cycle at 95°C for 30 s; one cycle at 50°C for 2 min and 95°C for 10 min; 40 cycles at 95°C for 1 min and 60°C for 1 min; one cycle at 95°C for 1 min and 55°C for 1 min; finally 80 cycles from 55 to 94.5°C, with a 0.5°C increment every 10 s to obtain a melting curve. Results were analyzed with the iQ5 software (BioRad). The nuclear gene encoding actin (accession AB158612) and the mitochondrial gene encoding RPL2 (accession BA000042, region 361 051–363 948) showed the most stable expression in our assays according to geNorm (38) and were taken as reference genes with the couples of primers ACTIN-1FW/ACTIN-1RV and RPL2-1FW/RPL2-1RV (Supplementary Data and Supplementary Table S1).

FLOE and 5′-RACE

Primer sequences are given in Supplementary Data and Supplementary Table S1. For fluorescently labeled oligonucleotide extension [FLOE (39)], 5 µg of mitochondrial RNA were used for extended SuperScript III reverse transcription with 5 nmol of the atp9tot3P-ROX reverse primer labeled at the 5′-end with 6-carboxy-X-rhodamine (ROX). After RNase A digestion, the cDNAs were ethanol precipitated, redissolved in water and completed with 8 µl of 1000 times diluted GeneScan 500 ROX fluorescent size standard (Applied Biosystems). Samples were finally analyzed with a capillary electrophoresis sequencer (Applied Biosystems).

5′-Rapid amplification of cDNA ends (5′-RACE) was carried out with the GeneRacer kit (Invitrogen). After ligation with the provided RNA primer, reverse transcription was run with SuperScript III and the atp9tot3P reverse primer. The final PCR involved the same primer and the Generacer5P direct primer corresponding to the sequence added through ligation. PCR products were analyzed on agarose gels, cloned into the pCR2.1-TOPO vector (Invitrogen) and sequenced.

Further RNA analyses

RNase protection was run according to Goodall *et al.* (40). [^{32}P]-labeled antisense probes and unlabeled sense transcripts were synthesized *in vitro* from appropriate templates with T7 RNA polymerase and a RiboMAX kit (Promega). Antisense hybridization was run overnight. Final products after RNase digestion were fractionated on denaturing polyacrylamide gels and visualized by autoradiography. Northern blot analyses were carried out following standard protocols with digoxigenin-labeled probes (Roche).

In organello protein synthesis

Mitochondria corresponding to 100 µg protein were incubated for 1 h at 25°C in 100 µl of IS buffer (5 mM KH$_2$PO$_4$, 300 mM mannitol, 60 mM KCl, 50 mM HEPES pH 7.0, 10 mM MgCl$_2$, 10 mM sodium malate, 10 mM NADH) completed with 2 mM GTP, 4 mM ADP, 2 mM DTT, 0.1% w/v BSA, 25 µM of each amino acid except methionine and 20–50 µCi [^{35}S]methionine (>800 Ci/mmol). The reactions were stopped upon addition of 1 ml washing buffer (300 mM sucrose, 10 mM K$_2$HPO$_4$, 1 mM EDTA, 5 mM glycine, 0.1% w/v BSA, pH 7.5) containing 10 mM unlabeled methionine. The samples were then centrifuged for 5 min at 12 000g to collect the organelles. Final mitochondrial pellets were analyzed by SDS polyacrylamide gel electrophoresis (SDS–PAGE) and fluorography according to standard protocols.

RESULTS

A mitochondrial translocation vector

We showed earlier that a bean (*Phaseolus vulgaris*) tRNA^{Leu} expressed from a nuclear transgene and carrying a 4-bp insertion in the anticodon loop was recovered in the mitochondria of transformed potato (*Solanum tuberosum*) plants (41). However, insertion of longer sequences was not successful. Grafting the 'passenger' RNA to the 5′-end of the tRNA^{Leu} as a trailor sequence also failed, due to RNase P removal of the extra sequence. We thus developed the use of a tRNA mimic as a mitochondrial import vector and selected the TLS formed by the last 82 nt at the 3′-end of the *Turnip yellow mosaic virus* (TYMV) genomic RNA (42). Mitochondrially imported tRNAs in higher plants include valine isoacceptors (43) and the TYMV TLS (Figure 1a) is an efficient tRNA^{Val} mimic. Its sequence does not comply with the consensus RNA polymerase III internal promoters, making easy a polymerase II-driven expression, and it does not seem to be processed by RNase P in plant cells. Finally, using an *in vitro* system (44), we showed that the TYMV TLS can be imported into isolated plant mitochondria with an efficiency and an ATP-dependence similar to those of a regular tRNA (Supplementary Data and Supplementary Figure S1). A pseudoknot (UPSK) upstream of the TLS in the TYMV genomic RNA contributes to optimized function in 3′ translational enhancement, which is dependent on aminoacylation (42); mitochondrial import of tRNAs in plant cells likewise seems to depend on interaction with the aminoacyl-tRNA synthetase (36,45). Thus, the tRNA mimic taken as a mitochondrial translocation vector consisted of the last 120 nt from the 3′-end of the
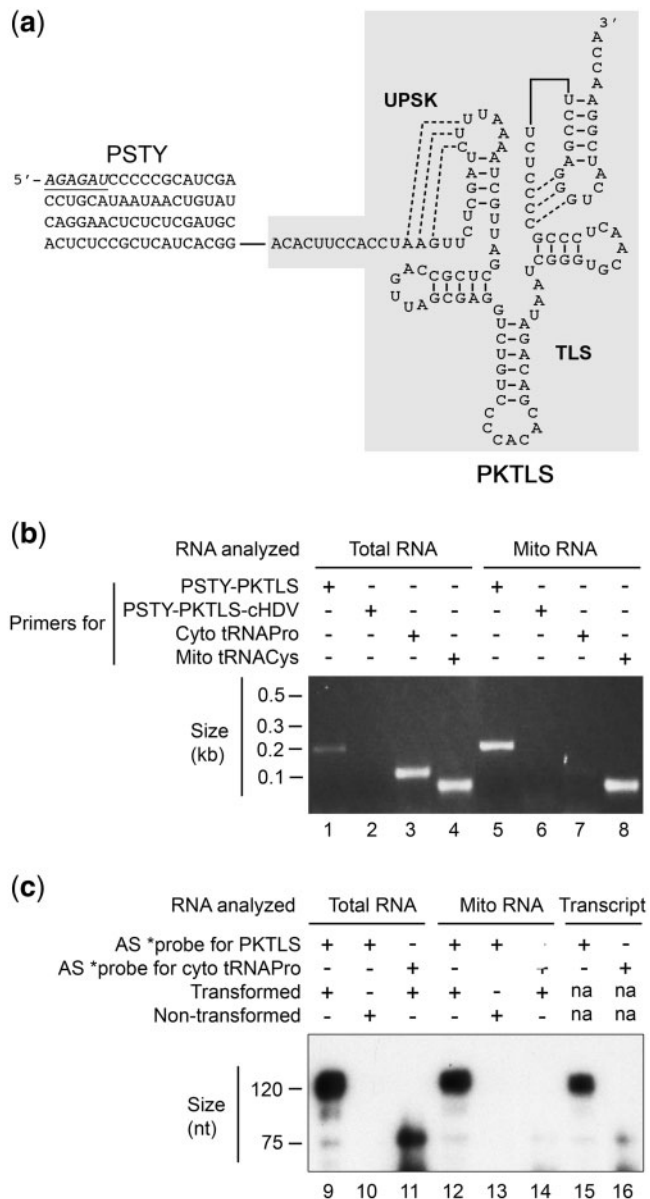
Figure 1. Mitochondrial import of a nuclear transgene-encoded passenger sequence in *N. tabacum* cells. (**a**) The PSTY-PKTLS RNA used to validate *in vivo* mitochondrial translocation. The PSTY passenger sequence, with six additional nucleotides (underlined and in italics) transcribed from the pBI-PSTYPKTLScHDV plasmid (see 'Materials and Methods' section), is attached to the 5′-end of the PKTLS composed of the TLS and upstream pseudoknot (UPSK). Base pairs forming pseudoknots are shown as dashed lines. (**b**) RT–PCR assays carried out with total or mitochondrial (Mito) RNA from transgenic *N. tabacum* cells expressing the PSTY-PKTLS-cHDV RNA. cDNA was synthesized with a reverse primer designed to amplify either the PSTY-PKTLS sequence (TLS3P) or the complete PSTY-PKTLS-cHDV sequence (HDV3P), in case self-cleavage of the cHDV would not have occurred. Subsequent PCR was run with primer TLS3P or HDV3P and a direct primer corresponding to the 5′-end of PSTY (PS5P). Amplification of the cytosolic tRNAs[Pro] (Cyto tRNAPro) with primers PRO5P and PRO3P served as a contamination control for the mitochondrial fraction. Primers CYS5P and CYS3P for mitochondrial tRNA[Cys] (GCA) (Mito tRNACys) were used to confirm the identity of the mitochondrial fraction. (**c**) RNase protection assays carried out with total or mitochondrial RNA from transgenic *N. tabacum* cells expressing the PSTY-PKTLS-cHDV RNA using *in vitro* synthesized antisense probes for PKTLS or cytosolic tRNAs[Pro]. RNA preparations from non-transformed cells served as

TYMV genomic RNA, including the TLS and the UPSK. This sequence will be called 'PKTLS' (Figure 1a).

Mitochondrial import of trailor RNAs

The strategy we developed for nuclear expression and mitochondrial import of RNAs of interest in plant cells is summarized in Figure 2. Plant cells are nuclearly transformed with constructs encoding a passenger sequence attached to the 5′-end of the TYMV PKTLS. These sequences are under the control of an RNA polymerase II promoter (constitutive or inducible) and terminator, yielding polyadenylated transcripts. To generate RNAs with the aminoacylatable TYMV TLS at the 3′-end, the sequence encoding the *cis*-cleaving ribozyme of the *Hepatitis delta virus* (cHDV) (27) is inserted into the constructs between the TYMV PKTLS cDNA and the terminator. Expression of the nuclear transgene thus generates a 5′-capped transcript comprising, successively, the passenger RNA, the PKTLS, the cHDV and the poly(A) tail. Self-cleavage of the cHDV eliminates the poly(A) tail and releases the regular 3′-CCA end of the PKTLS. The passenger RNA associated with the PKTLS is then exported from the nucleus to the cytosol, presumably recognized by the mitochondrial tRNA import machinery and finally imported into the organelles.

We first took as a passenger sequence the 66 nt located immediately upstream (positions 6134–6199) of the PKTLS (positions 6200–6318, plus a 3′-A) in the TYMV genomic RNA (Figure 1a, PSTY). The expected functionality of the PSTY-PKTLS RNA was assessed by establishing the capacity of the corresponding *in vitro*-synthesized transcript to be aminoacylated with valine in the presence of enzymatic extracts from *N. tabacum* BY-2 cell suspensions (Supplementary Data and Supplementary Figure S2a). According to the above strategy (Figure 2), the sequences encoding the PSTY passenger, the PKTLS translocation vector and the cHDV were assembled under the control of the CaMV 35S promoter in the pBI101 plasmid. The construct was used for nuclear transformation of *N. tabacum* BY-2 cells.

Total and mitochondrial RNAs were prepared from transformant cells harvested at mid-exponential growth phase. RT–PCR with the corresponding primers showed the presence of the PSTY-PKTLS RNA in the total RNA fraction and in the mitochondrial RNA fraction (Figure 1b, lanes 1 and 5). The identity of the RT–PCR products was confirmed by cloning and sequencing. Control reactions assessed the specificity of the amplifications and the absence of significant cytosolic contamination of the mitochondrial fractions. Self-cleavage of the cHDV was demonstrated by the absence of amplification products in reactions involving the corresponding reverse primer (Figure 1b, lanes 2 and 6). Accuracy of cHDV self-cleavage was confirmed by CR–RT–PCR, with

Figure 1. Continued

controls. Assays with *in vitro*-synthesized sense transcripts (lanes 15 and 16) yielded reference products. Marker sizes are indicated in kilobases (kb) or nucleotide numbers (nt). Primer sequences are given in Supplementary Data and Supplementary Table S1.
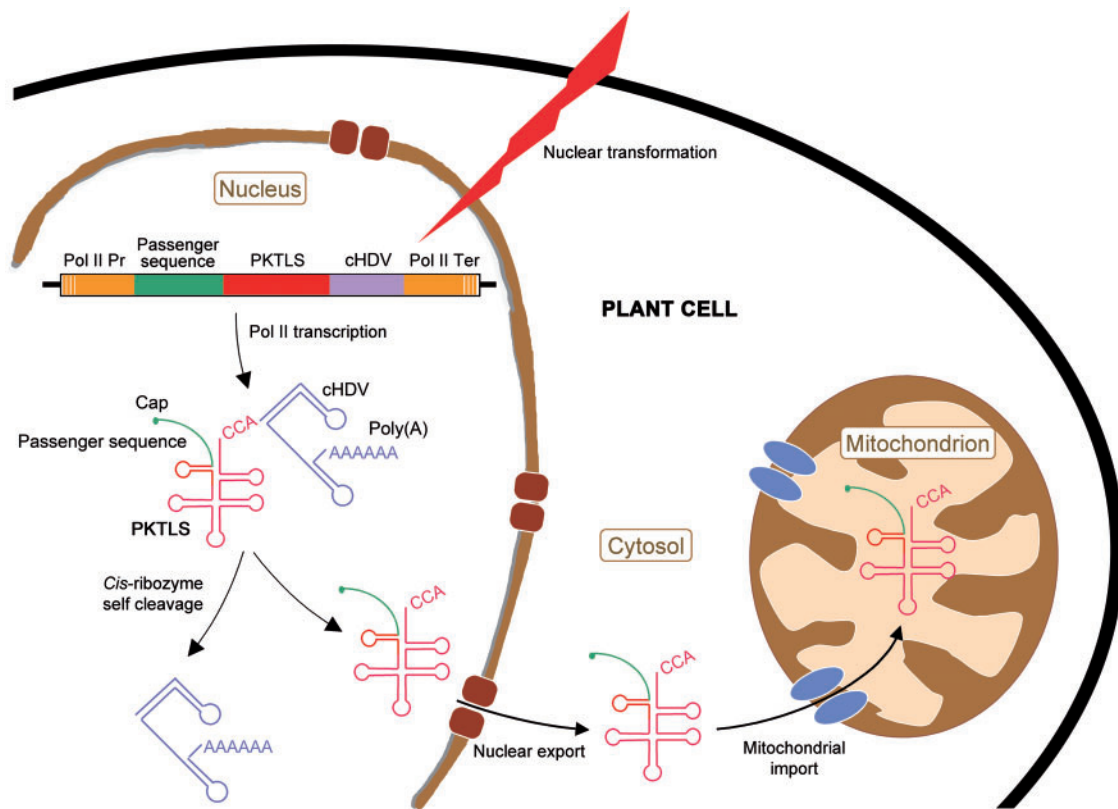
Figure 2. General scheme of the strategy developed for nuclear expression and mitochondrial import of RNAs of interest in plant cells. Description of the different steps is given in the text.

subsequent cloning and sequencing of the amplification products.

Total and mitochondrial RNA fractions from transformed cells were further analyzed through RNase protection assays using a radioactive probe complementary to the PKTLS. The results showed the protection of an antisense fragment of the expected size in the presence of either the total or the mitochondrial RNA fraction (Figure 1c, lanes 9 and 12). No fragment was protected in the presence of RNA fractions from untransformed cells (Figure 1c, lanes 10 and 13). Assays with a radioactive probe complementary to cytosol-specific tRNA^{Pro} again confirmed the absence of significant cytosolic contamination of the mitochondrial fractions (Figure 1c, lane 14). These experiments established that the PKTLS tRNA mimic was able to drive passenger RNAs into mitochondria.

Mitochondrial translocation and tRNA import specificity

The TYMV PKTLS mimics tRNA valine, a tRNA which is naturally imported into mitochondria in plant cells. To investigate whether the PSTY-PKTLS RNA was translocated into the organelles following the regular tRNA import pathway, we changed the aminoacylation specificity. Cytosolic tRNA^{Met} is not taken up by mitochondria in plant cells (43). In previous experiments (36), variants of an *Arabidopsis thaliana* cytosolic tRNA^{Val} carrying various mutations were expressed in tobacco cells from

transgenes. In line with the absence of cytosolic tRNA^{Met} in the natural set of organelle tRNAs, a mutant tRNA^{Val} possessing a methionine anticodon that switches the aminoacylation specificity from valine to methionine was not recovered in mitochondria (36).

A mutated TYMV TLS variant accepting methionine instead of valine was described previously (31). Based on these data, we designed PKTLSmet (Figure 3a) mimicking both a tRNA which is not naturally imported into plant mitochondria and the above-mentioned tRNA^{Val} mutant. PKTLSmet was in turn combined with the PSTY passenger sequence and expressed in *N. tabacum* cells following the strategy outlined in Figure 2. RT–PCR and RNase protection analyses (Figure 3b) showed the presence of the PSTY-PKTLSmet RNA in total RNA fractions from the transformants but not in mitochondrial RNA fractions (Figure 3b, lanes 1 and 4). Thus, the PSTY-PKTLSmet RNA was expressed but not imported into mitochondria. Aminoacylation assays showed that the *in vitro*-synthesized PSTY-PKTLSmet transcript had indeed lost the capacity to be valylated but could be charged with methionine (Supplementary Data and Supplementary Figure S2c). The lack of mitochondrial import of PSTY-PKTLSmet in the transformed cells was thus unlikely to be due to a lack of functionality of the RNA but, like in the case of the mutant tRNA^{Val}, rather reflected the change in amino acid specificity. Altogether, the data indicated that PKTLS-driven mitochondrial
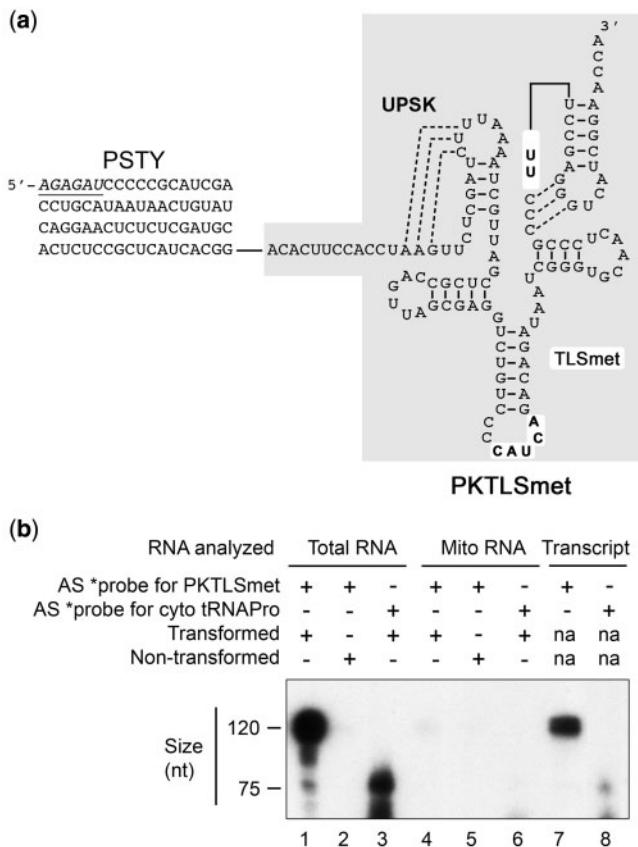
Figure 3. Mitochondrial import specificity of nuclear transgene-encoded passenger sequences in *N. tabacum* cells. (**a**) The PSTY-PKTLSmet RNA used to test the specificity of *in vivo* mitochondrial translocation. The structure is as in Figure 1a but the TLS moiety carries a methionine anticodon, two further nucleotide exchanges in the anticodon loop and 2 nt deletions in the L1 loop (bold on white background). (**b**) RNase protection assays carried out with total or mitochondrial RNA from transgenic *N. tabacum* cells expressing the PSTY-PKTLSmet-cHDV RNA using *in vitro* synthesized antisense probes for PKTLSmet or cytosolic tRNAs^Pro (contamination control). RNA preparations from non-transformed cells served as controls. Assays with *in vitro*-synthesized sense transcripts (lanes 7 and 8) yielded reference products. Marker sizes are indicated in nucleotide numbers (nt).

translocation followed the natural tRNA import specificity, suggesting a transport along the regular tRNA uptake pathway.

A chimeric *trans*-cleaving ribozyme

Demonstrating the flexibility of mitochondrial RNA translocation opened the way for functional and genetic manipulation of mitochondria in plant cells. As a further breakthrough, we developed specific knockdown of target RNAs in mitochondria, using as a passenger sequence of the PKTLS a *trans*-cleaving catalytic RNA, i.e. a hammerhead ribozyme. The *atp9* mRNA was chosen as a target. Knockdown of this major mitochondrial mRNA was of interest both to establish the efficiency of the approach and to initiate regulation studies. The main obstacle in applying hammerhead ribozymes *in vivo* is their requirement for much higher free magnesium concentrations

(10–25 mM) than those estimated to be present in cells [1–2 mM in plant mitochondria (46)]. We designed the *trans*-cleaving hammerhead ribozyme against the *atp9* mRNA (Rzatp9, Figure 4a) based on a shortened catalytic core derived from the results of *in vitro* selection for variants active in low magnesium conditions (47). Such ribozymes, with 2 instead of 4 bp in helix II and a UUUU tetraloop, showed high activity at very low Mg^{2+} concentration both *in vitro* and *in vivo* (48). The targeted site contained an AUC triplet, which is efficiently cleaved if placed in an appropriate sequence context (49). To ensure high specificity of the ribozyme, the antisense flanks responsible for target recognition and binding were designed to form 8 and 7 bp in helixes I and III, respectively (Figure 4a). The Rzatp9 ribozyme was attached to the 5′-end of the PKTLS through a specific 42-nt linker (L), to provide spacing and avoid alternative structures. The functionality of the PKTLS in the chimeric RNA was in turn assessed by establishing the capacity of the corresponding *in vitro*-synthesized transcript to be aminoacylated with valine in the presence of enzymatic extracts from *N. tabacum* BY-2 cell suspensions (Supplementary Data and Supplementary Figure S2b).

In vitro ribozyme cleavage activity

The catalytic activity of the Rzatp9 ribozyme alone or included in a T7 RNA polymerase-synthesized Rzatp9-L-PKTLS RNA was first assayed *in vitro* at various magnesium concentrations. A 100-nt long RNA corresponding to part of the *A. thaliana atp9* mRNA was used as a substrate (Figure 4b). Both Rzatp9 and Rzatp9-L-PKTLS ribozymes efficiently cleaved the target RNA at submillimolar Mg^{2+} concentrations (Figure 4c). Hydrolysis occurred at Mg^{2+} concentrations as low as 0.1 mM (Figure 4c, lane 8). Preparing the *in vivo* strategy, the activity of an extended Rzatp9-L-PKTLS RNA (extRzatp9-L-PKTLS, 5′-extension of 40 nt), representative for the full transcript expected upon expression from the pER8 vector [(33), see below], was assayed *in vitro* with a 146-nt-long target derived from *N. tabacum atp9* (Figure 4d and e). Again, an efficient cleavage was observed, even in the absence of added Mg^{2+} in the assay (Figure 4e, lane 17). Thus, a properly devised ribozyme/linker/PKTLS chimera retains high catalytic activity at physiological magnesium concentrations. Interestingly, additional sequences at both the 3′ and the 5′-end of the minimal Rzatp9 ribozyme not only did not reduce its catalytic activity, but seemed to enhance cleavage at low magnesium (Figure 4c and e).

Knockdown of a mitochondrial RNA in plant cells

The Rzatp9-, L-, PKTLS- and cHDV-encoding sequences were subsequently assembled under the control of the O_{LexA}-46 estradiol-inducible promoter in the pER8 vector (33) and used for nuclear transformation of *N. tabacum* BY-2 cells. Total and mitochondrial RNAs from induced transformant cells harvested at Day 4 after onset of estradiol treatment were tested as above by RT–PCR and RNase protection, demonstrating the expression and efficient mitochondrial import of the
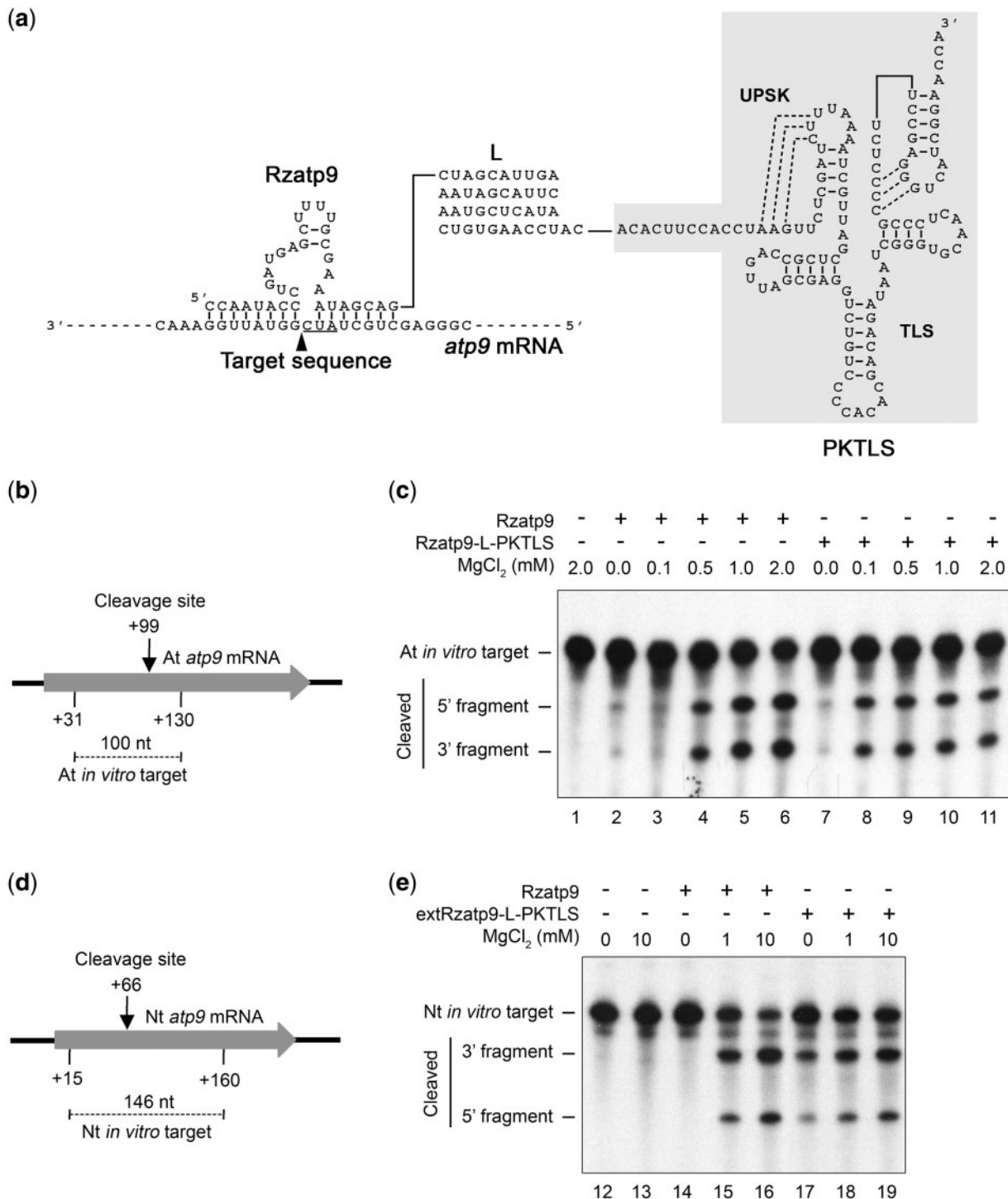
Figure 4. Structure and *in vitro trans*-cleaving activity of the Rzatp9-L-PKTLS chimeric RNA. (**a**) Structure of the Rzatp9-L-PKTLS RNA. The *trans*-cleaving ribozyme Rzatp9 directed against the *atp9* mRNA is attached to the 5′-end of the PKTLS via a 42-nt linker (L) selected from a pool of random sequences. The Rzatp9 hammerhead sequence is annealed to the target sequence motif in the *atp9* mRNA. The cleavage site is indicated by a black triangle. (**b**) Position of the target sequence (At *in vitro* target) used in (c) and of the Rzatp9 cleavage site in the *A. thaliana atp9*-coding sequence. (**c**) *Trans*-cleaving activity of the Rzatp9 hammerhead ribozyme alone and of the Rzatp9-L-PKTLS RNA as a function of Mg^{2+} concentration. A $[^{32}P]$-labeled target transcript derived from the *A. thaliana atp9*-coding sequence as indicated in (b) was incubated with *in vitro* synthesized Rzatp9 (lanes 2–6) or Rzatp9-L-PKTLS (lanes 7–11). Reactions were run for 2 h in standard conditions (see 'Materials and Methods' section). The ribozyme/target molar ratio was 10/1. (**d**) Position of the target sequence (Nt *in vitro* target) used in (e) and of the Rzatp9 cleavage site in the *N. tabacum atp9*-coding sequence. (**e**) *Trans*-cleaving activity of the Rzatp9 ribozyme alone and of the 5′-extended Rzatp9-L-PKTLS RNA expected from *in vivo* expression (extRzatp9-L-PKTLS) as a function of Mg^{2+} concentration. A $[^{32}P]$-labeled target transcript derived from the *N. tabacum atp9*-coding sequence as indicated in (d) was incubated with *in vitro* synthesized Rzatp9 (lanes 14–16) or extRzatp9-L-PKTLS (lanes 17–19). Reactions were run as in (c) for 3 h. Migration of the full-length targets and of the fragments generated upon cleavage is indicated by arrows.

Rzatp9-L-PKTLS RNA (Figure 5a and b). Expression of the chimeric ribozyme in estradiol-induced transformed cells was subsequently analyzed by real-time RT–PCR over a 1-week growth cycle. The Rzatp9-L-PKTLS level reached a plateau from Day 3 to Day 5 and decreased when approaching the stationary phase (Figure 6a). The same samples served in turn as real-time RT–PCR templates to assess the levels of the *atp9* mRNA. Control levels were established with RNA samples from uninduced transformed cells and from estradiol-treated wild-type cells. Estradiol showed a significant effect on RNA levels in wild-type cells. Accurate analysis was thus carried out by comparing the *atp9* mRNA levels in RNA samples from estradiol-treated transformant cells and estradiol-treated wild-type cells. We demonstrated that, after a lag phase, the *atp9* mRNA level dropped by 80% at Day 4 in induced transformant cells versus estradiol-treated wild-type cells (Figure 6b). Mitochondria isolated at Day 4 from uninduced and estradiol-induced transformant cells were used in turn for *in organello* translation assays in the presence of [^{35}S]methionine. Reflecting the drop in the
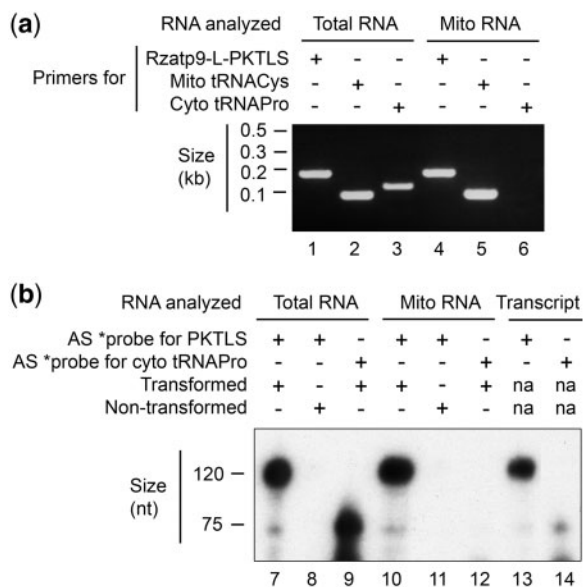

Figure 5. Mitochondrial import of the Rzatp9-L-PKTLS chimeric RNA in cell cultures. (**a**) RT–PCR assays carried out with total or mitochondrial (Mito) RNA prepared from *N. tabacum* cells transformed via pER8-Rzatp9LPKTLScHDV (see 'Materials and Methods' section), treated with estradiol and harvested at Day 4. cDNA was synthesized with the reverse primer TLS3P complementary to the 3′-end of PKTLS. Subsequent PCR was run with the direct primer Rzatp95P corresponding to the 5′-end of Rzatp9 and the reverse primer TLSmP complementary to an internal sequence close to the 3′-end of PKTLS (Supplementary Data and Supplementary Table S1). Amplification of cytosolic tRNAs^Pro (Cyto tRNAPro, contamination control) and mitochondrial tRNA^Cys(GCA) (Mito tRNACys, identity of the mitochondrial fraction) were as in Figure 1b. (**b**) RNase protection assays carried out with total or mitochondrial RNA from *N. tabacum* cells transformed via pER8-Rzatp9LPKTLScHDV, treated with estradiol and harvested at Day 4. *In vitro* synthesized antisense probes for PKTLS or cytosolic tRNAs^Pro were used. RNA preparations from non-transformed cells served as controls. Assays with *in vitro* synthesized sense transcripts (lanes 13 and 14) yielded reference products. Marker sizes are indicated in kilobases (kb) or nucleotide numbers (nt).
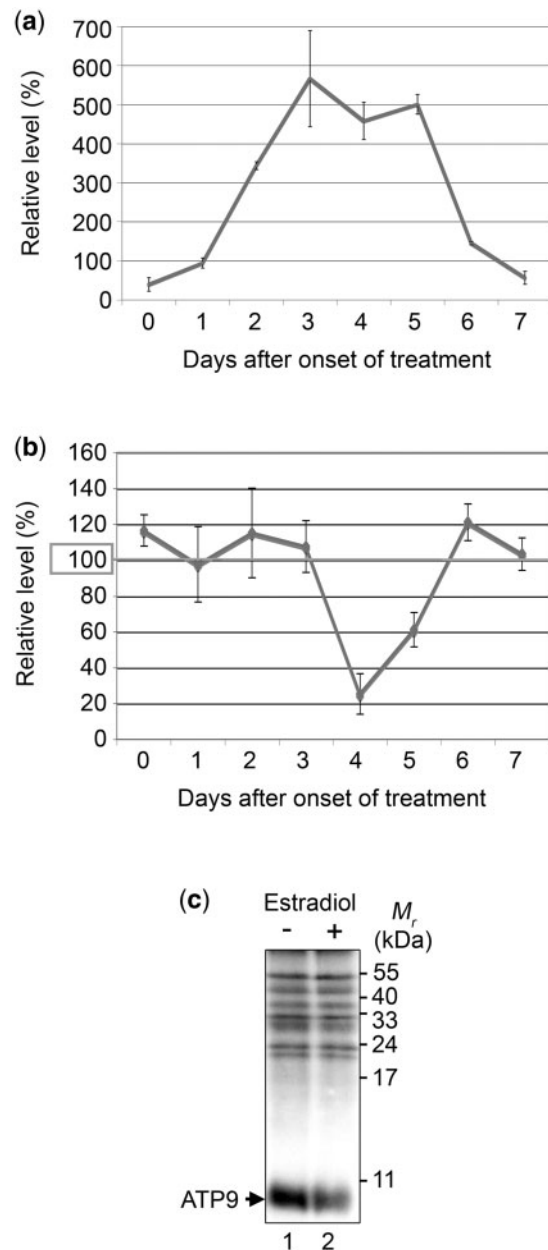

Figure 6. Expression of the Rzatp9-L-PKTLS RNA and target knockdown in cell cultures. (**a**) Relative expression of the Rzatp9-L-PKTLS RNA in *N. tabacum* cells transformed via the pER8-Rzatp9LPKTLScHDV plasmid (see 'Materials and Methods' section) and treated with estradiol. Cells were harvested every day over a 1-week culture period. Estradiol was added to the medium at the beginning of the culture. Total RNA was prepared from all samples and cDNA was synthesized with a random hexanucleotide mixture. The cDNA served as a template for real-time PCR analysis with the direct primer RZATP9-TLS-FW specific for Rzatp9 and the reverse primer RZATP9-TLS-RV specific for the PKTLS (Supplementary Data and Supplementary Table S1). (**b**) Relative level of the *atp9* mRNA in *N. tabacum* cells transformed via pER8-Rzatp9LPKTLScHDV and treated with estradiol. The cDNA samples from (a) served in turn as templates for real-time PCR analysis with primers ATP9-1-66NT-FW and ATP9-1-66NT-RV (Supplementary Data and Supplementary Table S1) specific for the *atp9* sequence. (**c**) *In organello* protein synthesis with [^{35}S]methionine in mitochondria isolated from *N. tabacum* cells transformed via pER8-Rzatp9LPKTLScHDV, untreated or treated with estradiol and harvested at Day 4. Migration of ATP9, as established with purified protein obtained through chloroform/methanol extraction, is indicated by an arrow.

atp9 mRNA level, synthesis of the ATP9 protein was reduced by ∼40% in mitochondria from induced transformant cells (Figure 6c). Only translation of the ATP9 protein was affected, underlining the specificity of the process. The absence of non-specific effects was further supported by proteomic analyses (Supplementary Data and Supplementary Figure S3). Observations from *in organello* translation assays also confirmed that the *atp9* mRNA was knocked down inside the organelles.

That the drop in *atp9* mRNA level resulted from ribozyme cleavage was shown by fluorescently labeled oligonucleotide extension [FLOE (39)] and 5′-RACE-PCR. FLOE assays with a 3′ primer and mitochondrial RNA samples from uninduced transformed cells harvested after 4 days of subculturing detected a 357-nt precursor of the *atp9* mRNA and a 244-nt mature form (Figure 7a and b). Levels of these products were reduced when analyzing mitochondrial RNA samples from estradiol-treated transformed cells harvested at the same stage, and a new signal appeared corresponding to the 168-nt 3′ fragment expected upon ribozyme cleavage of the *atp9* mRNA (Figure 7a and c). This fragment was specific for mitochondrial RNA from induced transformant cells. A minor primer extension product of only 133 nt was also detected in the FLOE pattern from cells expressing the Rzatp9-L-PKTLS RNA (Figure 7c). The *atp9* sequence at that distance from the 3′ end offers no possibility for ribozyme annealing and cleavage. The 133-nt fragment might thus represent some secondary intermediate generated by the mitochondrial RNA degradation system following the initial cleavage mediated by the imported chimeric ribozyme. 5′-RACE–PCR assays involving the same 3′ primer also detected the 168-nt fragment, as well as the fragments representative for the precursor and processed *atp9* mRNA. Cloning/sequencing confirmed the identity of all products.

Worthy to notice, RNA samples from induced transformant cells at Day 3 already contained highest levels of Rzatp9-L-PKTLS but retained normal *atp9* mRNA levels (Figure 6a and b). This further excluded that the *atp9* drop observed with samples from Days 4 and 5 be due to target cleavage during RNA extraction and handling. Thus, the results altogether demonstrated that the Rzatp9-L-PKTLS chimeric ribozyme expressed from a nuclear transgene was imported into mitochondria and specifically cleaved its target RNA at the expected position, triggering a strong knockdown. These observations establish that appropriate *trans*-cleaving ribozymes are active in the organelles.

Mitochondrial RNA knockdown in whole plants

The pER8 plasmid carrying the Rzatp9-L-PKTLS-cHDV construct was used in turn to generate stable *A. thaliana* transgenic plants. When the expression of the Rzatp9-L-PKTLS RNA was induced in fully developed plants (Figure 8a) cultivated under long day conditions (16 h light/8 h dark), the *atp9* mRNA dropped to a very low level, as revealed by northern blot analysis (Figure 8b). The knockdown persisted when the induction was maintained through regular estradiol treatment. No dramatic change in phenotype was observed over a period of
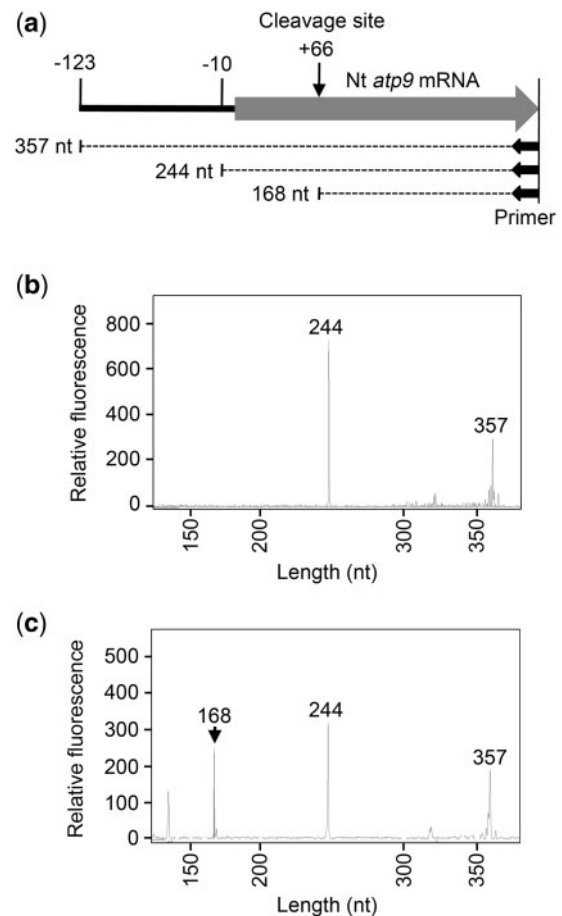

Figure 7. *In vivo* cleavage of the mitochondrial *atp9* mRNA. (**a**) Scheme illustrating the products expected from fluorescently labeled oligonucleotide extension (FLOE, see 'Materials and Methods' section) of the *atp9* precursor (357 nt), mature form (244 nt) and 3′ fragment upon ribozyme cleavage (168 nt), using the atp9tot3P-ROX primer (Supplementary Data and Supplementary Table S1). Sizes of the precursor and mature form were established by FLOE experiments with RNA from wild-type *N. tabacum* cells and proved consistent with the *atp9* promoter data in *Solanum tuberosum* (62). (**b**) and (**c**) *atp9* FLOE analysis of total RNA from *N. tabacum* cells transformed via the pER8-Rzatp9LPKTLScHDV plasmid (see 'Materials and Methods' section), untreated (b) or treated with estradiol (c) and harvested at Day 4. The expected FLOE product representative for the 168-nt 3′ fragment resulting from ribozyme cleavage is indicated by an arrow.

12 days, suggesting that in such a context where the requirement for mitochondrial activity is moderate, the turnover of the ATP9 protein is slow and the *atp9* mRNA in excess. Nevertheless, also in younger plants (Figure 8c) maintained in short day conditions (8 h light/16 h dark) induced expression of the Rzatp9-L-PKTLS RNA led to a strong and persistent *atp9* knockdown (Figure 8d). On the other hand, expressing the Rzatp9-L-PKTLS RNA in very young plantlets (Figure 8e) grown under short day conditions yielded transient *atp9* knockdown (Figure 8f). The latter observation suggests that, when the demand for mitochondrial activity is high, the drop in *atp9* level can be sensed and possibly trigger increased synthesis. It can be noticed that also in exponentially growing *N. tabacum* cells, *atp9* knockdown is partially released at Day 5,
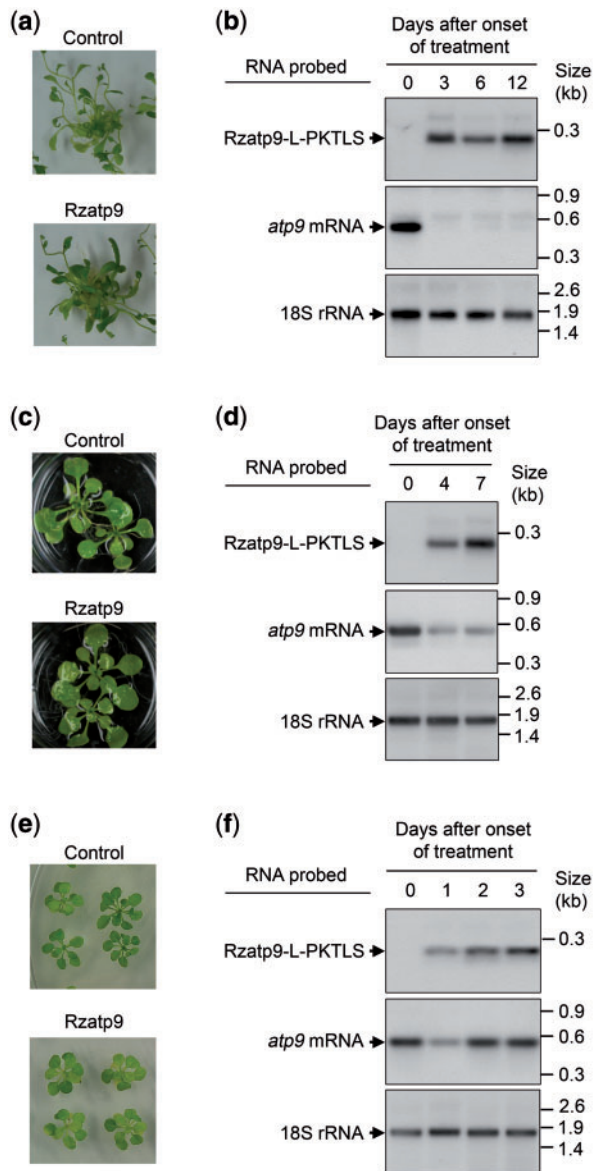
Figure 8. Expression of the Rzatp9-L-PKTLS RNA and target knockdown in *A. thaliana* plants stably transformed via the pER8-Rzatp9LPKTLScHDV plasmid (see 'Materials and Methods' section). Mature plants cultivated under long day conditions (16 h light/8 h dark) (**a**), developing plants cultivated under short day conditions (8 h light/16 h dark) (**c**) and very young plantlets cultivated under short day conditions (**e**) were treated with estradiol for various times to induce and maintain the expression of the transgene (Rzatp9). Fresh estradiol-containing medium was added every 3–4 days. Plants were harvested at different time points and total RNA was extracted from all samples. The expression of the Rzatp9-L-PKTLS RNA and the *atp9* mRNA level were analyzed by northern blotting (**b**, **d** and **f**). The 18S rRNA served as a control. Migration of size marker RNAs is indicated. The following couples of primers (Supplementary Data and Supplementary Table S1) were used to amplify the probes: ext5Pnor and TLS3P (probe for the Rzatp9-L-PKTLS RNA), atp9nor5P and atp9nor3P (probe for the *atp9* mRNA), 18Snor5P and 18Snor3P (probe for the 18S rRNA).

although the ribozyme is still at a high level (Figure 6a and b). Whereas it is currently considered that organelle gene expression is mostly constitutive, such observations are in favor of mRNA control mechanisms in mitochondria with

relation to the plant developmental stage and culture conditions. Knockdown of other organelle RNAs with specifically designed *trans*-cleaving ribozymes will allow further analysis of these processes. As a whole, the data demonstrate that our molecular approach is extremely efficient to knockdown mitochondrial RNAs in whole plants and has an important potential for the investigation of organelle regulation mechanisms.

DISCUSSION

The molecular strategy developed in this work brings a decisive breakthrough in the analysis and manipulation of mitochondrial genetic processes. So far, investigations on mitochondrial transcription, RNA processing, RNA stability and degradation or RNA editing had to rely mostly on reconstituted *in vitro* or *in organello* assays. Allowing the import of customized sense or antisense RNAs into the organelles, our results open the way for direct *in vivo* analyses. Around half of the sequences in plant mitochondrial genomes are of unknown origin and function (3). Unexpectedly, most of these sequences are transcribed (5). *Trans*-ribozyme-mediated knockdown of such transcripts will uncover new functional and/or regulatory properties of plant mitochondria. In particular, it will be of interest to look for putative RNA-mediated regulation mechanisms in organelles, as candidate non-coding RNAs have been identified in both mitochondria and chloroplasts (50–52).

Our chimeric hammerhead ribozyme variant was designed with a shorter core domain which differed from the natural hammerhead motif contained in the satellite RNA of *Tobacco ringspot virus* (53) in the length of helix II (2 bp instead of 4) and in the sequence of loop 2 (UUUU instead of GUGA) (Figure 4a), a structure previously shown to support *in vitro* activity at low magnesium concentration (47). This design indeed allowed a drastic drop of the target mRNA level in mitochondria, raising further interest for the use of *trans*-cleaving catalytic RNAs *in vivo*. Differing from this minimal concept, it has been demonstrated that sequence elements outside of the core structure of natural hammerhead ribozymes enable catalytic activity at physiological Mg^{2+} concentrations by facilitating and stabilizing the active conformation via tertiary interactions between terminal loops or internal bulges (54–56). Artificial tertiary stabilizing motifs (TSMs) supporting ribozyme *trans*-cleavage in sub-millimolar $MgCl_2$ were also identified through SELEX screening (57) and the observations were extended to different types of hammerhead ribozymes (58). In the present study, we favored the short core minimal concept with the view that it would be a better suited passenger RNA for mitochondrial import and would be less prone to generate structural conflicts with the PKTLS. Tertiary-stabilized ribozymes can be an alternative but the longer loop and the extended flank enabling the formation of a bulge upon annealing to the target RNA in turn enhance structural constraints, so that combination with the PKTLS might be more complex and affect mitochondrial import. On the other hand, it can be noted that the efficiency of the

minimal ribozyme used here was not affected by the additional 5′ sequence generated from the *in vivo* transcription unit or by the presence of the linker and PKTLS at the 3′-end, rather the presence of these sequences could contribute to increased RNA stability in the cells.

Properly designed hammerhead ribozymes are highly specific and off-target effects are considered as rare (59). To ensure specificity, the design of our ribozyme was elaborated according to previous functional data. It is known that the activity is significantly reduced if there are <14 bp between the ribozyme and the target RNA, whereas mismatches can be tolerated if the length of the complementary region is 18 bp or more (60). Increasing the length of the base-paired regions flanking the cleavage site beyond an optimal threshold was thus not considered as a factor improving specificity (61). The target-annealing arms in our ribozyme design provide a total of 15 bp (8 + 7). According to the available data, this ensures high specificity, as any mismatch will lead to a drop in activity and the probability of an alternative, perfectly matching sequence is extremely low. In particular, the ribozyme targeted against the *atp9* mRNA has no alternative candidate cleavage site in the whole *N. tabacum* or *A. thaliana* mitochondrial genome. In the *A. thaliana* nuclear genome, the only matching sequence is that of the *atp9* gene copy in the large mitochondrial DNA insertion found in chromosome 2.

As it is possible to design specific hammerhead ribozymes to target virtually any RNA, such a strategy could become a universal approach for both fundamental studies of mitochondrial gene functions and for biotechnologies involving the manipulation of organelle gene expression. For example, breeding of major crops still needs the development of new strategies for rapid and easy generation of CMS lines. The approach described here has the potential to provide male sterile lines through either the knockdown of a mitochondrial RNA or the organelle import and translation of RNAs normally found in CMS lines.

Allotopic expression and organelle import of customized RNAs offers a further important advantage, even over a still unfeasible mitochondrial genetic transformation, which is the versatility of nuclear promoters. The latter will allow regulatable genetic manipulation of the organelles, using an inducible promoter, or restriction of the strategy with a tissue-specific promoter. Finally, since tRNA import into mitochondria is a common phenomenon (24,25), the approach may prove to be suitable in many organisms, including humans.

SUPPLEMENTARY DATA

Supplementary Data are available at NAR Online.

ACKNOWLEDGEMENTS

REFERENCES

1. Montoya,J., Gaines,G.L. and Attardi,G. (1983) The pattern of transcription of the human mitochondrial rRNA genes reveals two overlapping transcription units. *Cell*, **34**, 151–159.
2. Fernandez-Silva,P., Enriquez,J.A. and Montoya,J. (2003) Replication and transcription of mammalian mitochondrial DNA. *Exp. Physiol.*, **88**, 41–56.
3. Kubo,T. and Newton,K.J. (2008) Angiosperm mitochondrial genomes and mutations. *Mitochondrion*, **8**, 5–14.
4. Bonen,L. (2008) *Cis-* and *trans-*splicing of group II introns in plant mitochondria. *Mitochondrion*, **8**, 26–34.
5. Holec,S., Lange,H., Canaday,J. and Gagliardi,D. (2008) Coping with cryptic and defective transcripts in plant mitochondria. *Biochim. Biophys. Acta*, **1779**, 566–573.
6. Takenaka,M., Verbitskiy,D., van der Merwe,J.A., Zehrmann,A. and Brennicke,A. (2008) The process of RNA editing in plant mitochondria. *Mitochondrion*, **8**, 35–46.
7. Rhoads,D.M. and Subbaiah,C.C. (2007) Mitochondrial retrograde regulation in plants. *Mitochondrion*, **7**, 177–194.
8. Pesaresi,P., Schneider,A., Kleine,T. and Leister,D. (2007) Interorganellar communication. *Curr. Opin. Plant Biol.*, **10**, 600–606.
9. Giraud,E., Van Aken,O., Ho,L.H. and Whelan,J. (2009) The transcription factor ABI4 is a regulator of mitochondrial retrograde expression of ALTERNATIVE OXIDASE1a. *Plant Physiol.*, **150**, 1286–1296.
10. Tuppen,H.A., Blakely,E.L., Turnbull,D.M. and Taylor,R.W. (2010) Mitochondrial DNA mutations and human disease. *Biochim. Biophys. Acta*, **1797**, 113–128.
11. Chase,C.D. (2007) Cytoplasmic male sterility: a window to the world of plant mitochondrial-nuclear interactions. *Trends Genet.*, **23**, 81–90.
12. Frei,U., Peiretti,E.G. and Wenzel,G. (2004) In Janick,J. (ed.), *Plant Breeding Reviews*, Vol. 23. John Wiley & Sons, Hoboken, pp. 175–210.
13. Mackenzie,S.A. (2005) In Janick,J. (ed.), *Plant Breeding Reviews*, Vol. 25. John Wiley & Sons, Hoboken, pp. 115–138.
14. Atienza,S.G., Martin,A.C., Ramirez,M.C., Martin,A. and Ballesteros,J. (2007) Effects of *Hordeum chilense* cytoplasm on agronomic traits in common wheat. *Plant Breeding*, **126**, 5–8.
15. Boynton,J.E., Gillham,N.W., Harris,E.H., Hosler,J.P., Johnson,A.M., Jones,A.R., Randolph-Anderson,B.L., Robertson,D., Klein,T.M., Shark,K.B. *et al.* (1988) Chloroplast transformation in *Chlamydomonas* with high velocity microprojectiles. *Science*, **240**, 1534–1538.
16. Svab,Z., Hajdukiewicz,P. and Maliga,P. (1990) Stable transformation of plastids in higher plants. *Proc. Natl Acad. Sci. USA*, **87**, 8526–8530.
17. Staub,J.M. and Maliga,P. (1995) Marker rescue from the *Nicotiana tabacum* plastid genome using a plastid/*Escherichia coli* shuttle vector. *Mol. Gen. Genet.*, **249**, 37–42.
18. Maliga,P. (2004) Plastid transformation in higher plants. *Annu. Rev. Plant Biol.*, **55**, 289–313.
19. Bock,R. (2007) Plastid biotechnology: prospects for herbicide and insect resistance, metabolic engineering and molecular farming. *Curr. Opin. Biotechnol.*, **18**, 100–106.
20. Daniell,H., Singh,N.D., Mason,H. and Streatfield,S.J. (2009) Plant-made vaccine antigens and biopharmaceuticals. *Trends Plant Sci.*, **14**, 669–679.

21. Wang,H.H., Yin,W.B. and Hu,Z.M. (2009) Advances in chloroplast engineering. *J. Genet. Genomics*, **36**, 387–398.
22. Bonnefoy,N., Remacle,C. and Fox,T.D. (2007) Genetic transformation of *Saccharomyces cerevisiae* and *Chlamydomonas reinhardtii* mitochondria. *Methods Cell Biol.*, **80**, 525–548.
23. Zhou,J., Liu,L. and Chen,J. (2010) Mitochondrial DNA heteroplasmy in *Candida glabrata* after mitochondrial transformation. *Eukaryot. Cell*, **9**, 806–814.
24. Salinas,T., Duchêne,A.M. and Maréchal-Drouard,L. (2008) Recent advances in tRNA mitochondrial import. *Trends Biochem. Sci.*, **33**, 320–329.
25. Alfonzo,J.D. and Söll,D. (2009) Mitochondrial tRNA import–the challenge to understand has just begun. *Biol. Chem.*, **390**, 717–722.
26. Mathews,D.H., Sabina,J., Zuker,M. and Turner,D.H. (1999) Expanded sequence dependence of thermodynamic parameters improves prediction of RNA secondary structure. *J. Mol. Biol.*, **288**, 911–940.
27. Perrotta,A.T. and Been,M.D. (1991) A pseudoknot-like structure required for efficient self-cleavage of hepatitis delta virus RNA. *Nature*, **350**, 434–436.
28. Weiland,J.J. and Dreher,T.W. (1989) Infectious TYMV RNA from cloned cDNA: effects *in vitro* and *in vivo* of point substitutions in the initiation codons of two extensively overlapping ORFs. *Nucleic Acids Res.*, **17**, 4675–4687.
29. Carrington,J.C., Freed,D.D. and Leinicke,A.J. (1991) Bipartite signal sequence mediates nuclear translocation of the plant potyviral NIa protein. *Plant Cell*, **3**, 953–962.
30. Heim,R., Cubitt,A.B. and Tsien,R.Y. (1995) Improved green fluorescence. *Nature*, **373**, 663–664.
31. Dreher,T.W., Tsai,C.H. and Skuzeski,J.M. (1996) Aminoacylation identity switch of *turnip yellow mosaic virus* RNA from valine to methionine results in an infectious virus. *Proc. Natl Acad. Sci. USA*, **93**, 12212–12216.
32. van Engelen,F.A., Molthoff,J.W., Conner,A.J., Nap,J.P., Pereira,A. and Stiekema,W.J. (1995) pBINPLUS: an improved plant transformation vector based on pBIN19. *Transgenic Res.*, **4**, 288–290.
33. Zuo,J., Niu,Q.W. and Chua,N.H. (2000) Technical advance: An estrogen receptor-based transactivator XVE mediates highly inducible gene expression in transgenic plants. *Plant J.*, **24**, 265–273.
34. An,G. (1985) High efficiency transformation of cultured tobacco cells. *Plant Physiol.*, **79**, 568–570.
35. Clough,S.J. and Bent,A.F. (1998) Floral dip: a simplified method for *Agrobacterium*-mediated transformation of *Arabidopsis thaliana*. *Plant J.*, **16**, 735–743.
36. Delage,L., Duchêne,A.M., Zaepfel,M. and Maréchal-Drouard,L. (2003) The anticodon and the D-domain sequences are essential determinants for plant cytosolic tRNA(Val) import into mitochondria. *Plant J.*, **34**, 623–633.
37. Ramakers,C., Ruijter,J.M., Deprez,R.H. and Moorman,A.F. (2003) Assumption-free analysis of quantitative real-time polymerase chain reaction (PCR) data. *Neurosci. Lett.*, **339**, 62–66.
38. Vandesompele,J., De Preter,K., Pattyn,F., Poppe,B., Van Roy,N., De Paepe,A. and Speleman,F. (2002) Accurate normalization of real-time quantitative RT-PCR data by geometric averaging of multiple internal control genes. *Genome Biol.*, **3**, RESEARCH0034.
39. Lloyd,A.L., Marshall,B.J. and Mee,B.J. (2005) Identifying cloned *Helicobacter pylori* promoters by primer extension using a FAM-labelled primer and GeneScan analysis. *J. Microbiol. Methods*, **60**, 291–298.
40. Goodall,G.J., Wiebauer,K. and Filipowicz,W. (1990) Analysis of pre-mRNA processing in transfected plant protoplasts. *Methods Enzymol.*, **181**, 148–161.
41. Small,I., Maréchal-Drouard,L., Masson,J., Pelletier,G., Cosset,A., Weil,J.H. and Dietrich,A. (1992) *In vivo* import of a normal or mutagenized heterologous transfer RNA into the mitochondria of transgenic plants: towards novel ways of influencing mitochondrial gene expression? *EMBO J.*, **11**, 1291–1296.
42. Matsuda,D. and Dreher,T.W. (2004) The tRNA-like structure of Turnip yellow mosaic virus RNA is a 3′-translational enhancer. *Virology*, **321**, 36–46.
43. Maréchal-Drouard,L., Guillemaut,P., Cosset,A., Arbogast,M., Weber,F., Weil,J.H. and Dietrich,A. (1990) Transfer RNAs of potato (*Solanum tuberosum*) mitochondria have different genetic origins. *Nucleic Acids Res.*, **18**, 3689–3696.
44. Delage,L., Dietrich,A., Cosset,A. and Maréchal-Drouard,L. (2003) *In vitro* import of a nuclearly encoded tRNA into mitochondria of *Solanum tuberosum*. *Mol. Cell. Biol.*, **23**, 4000–4012.
45. Dietrich,A., Maréchal-Drouard,L., Carneiro,V., Cosset,A. and Small,I. (1996) A single base change prevents import of cytosolic tRNA(Ala) into mitochondria in transgenic plants. *Plant J.*, **10**, 913–918.
46. Igamberdiev,A.U. and Kleczkowski,L.A. (2001) Implications of adenylate kinase-governed equilibrium of adenylates on contents of free magnesium in plant cells and compartments. *Biochem. J.*, **360**, 225–231.
47. Persson,T., Hartmann,R.K. and Eckstein,F. (2002) Selection of hammerhead ribozyme variants with low Mg2+ requirement: importance of stem-loop II. *Chembiochem.*, **3**, 1066–1071.
48. Fedoruk-Wyszomirska,A., Szymanski,M., Wyszko,E., Barciszewska,M.Z. and Barciszewski,J. (2009) Highly active low magnesium hammerhead ribozyme. *J. Biochem.*, **145**, 451–459.
49. Zoumadakis,M. and Tabler,M. (1995) Comparative analysis of cleavage rates after systematic permutation of the NUX consensus target motif for hammerhead ribozymes. *Nucleic Acids Res.*, **23**, 1192–1196.
50. Lung,B., Zemann,A., Madej,M.J., Schuelke,M., Techritz,S., Ruf,S., Bock,R. and Huttenhofer,A. (2006) Identification of small non-coding RNAs from mitochondria and chloroplasts. *Nucleic Acids Res.*, **34**, 3842–3852.
51. Madej,M.J., Alfonzo,J.D. and Huttenhofer,A. (2007) Small ncRNA transcriptome analysis from kinetoplast mitochondria of *Leishmania tarentolae*. *Nucleic Acids Res.*, **35**, 1544–1554.
52. Marker,C., Zemann,A., Terhorst,T., Kiefmann,M., Kastenmayer,J.P., Green,P., Bachellerie,J.P., Brosius,J. and Huttenhofer,A. (2002) Experimental RNomics: identification of 140 candidates for small non-messenger RNAs in the plant *Arabidopsis thaliana*. *Curr. Biol.*, **12**, 2002–2013.
53. Nelson,J.A., Shepotinovskaya,I. and Uhlenbeck,O.C. (2005) Hammerheads derived from sTRSV show enhanced cleavage and ligation rate constants. *Biochemistry*, **44**, 14577–14585.
54. Khvorova,A., Lescoute,A., Westhof,E. and Jayasena,S.D. (2003) Sequence elements outside the hammerhead ribozyme catalytic core enable intracellular activity. *Nat. Struct. Biol.*, **10**, 708–712.
55. De la Pena,M., Gago,S. and Flores,R. (2003) Peripheral regions of natural hammerhead ribozymes greatly increase their self-cleavage activity. *EMBO J.*, **22**, 5561–5570.
56. Penedo,J.C., Wilson,T.J., Jayasena,S.D., Khvorova,A. and Lilley,D.M. (2004) Folding of the natural hammerhead ribozyme is enhanced by interaction of auxiliary elements. *RNA*, **10**, 880–888.
57. Saksmerprome,V., Roychowdhury-Saha,M., Jayasena,S., Khvorova,A. and Burke,D.H. (2004) Artificial tertiary motifs stabilize *trans*-cleaving hammerhead ribozymes under conditions of submillimolar divalent ions and high temperatures. *RNA*, **10**, 1916–1924.
58. Burke,D.H. and Greathouse,S.T. (2005) Low-magnesium, *trans*-cleavage activity by type III, tertiary stabilized hammerhead ribozymes with stem 1 discontinuities. *BMC Biochem.*, **6**, 14.
59. Scherer,L.J. and Rossi,J.J. (2003) Approaches for the sequence-specific knockdown of mRNA. *Nat. Biotechnol.*, **21**, 1457–1465.
60. Ellis,J. and Rogers,J. (1993) Design and specificity of hammerhead ribozymes against calretinin mRNA. *Nucleic Acids Res.*, **21**, 5171–5178.
61. Hertel,K.J., Herschlag,D. and Uhlenbeck,O.C. (1996) Specificity of hammerhead ribozyme cleavage. *EMBO J.*, **15**, 3751–3757.
62. Lizama,L., Holuigue,L. and Jordana,X. (1994) Transcription initiation sites for the potato mitochondrial gene coding for subunit 9 of ATP synthase (atp9). *FEBS Lett.*, **349**, 243–248.